

Article

Nonlinear Seismic Response of Multistory Steel Frames with Self-Centering Tension-Only Braces

Pei Chi ^{1,*} , Jun Dong ², Wenlong Tian ¹ and Dafu Cao ¹

¹ College of Civil Science and Engineering, Yangzhou University, Yangzhou 225009, China; MX120170450@yzu.edu.cn (W.T.); dfcao@yzu.edu.cn (D.C.)

² College of Civil Engineering, Nanjing Tech University, Nanjing 211816, China; dongjun@njtech.edu.cn

* Correspondence: chipei@yzu.edu.cn

Received: 27 November 2019; Accepted: 3 March 2020; Published: 6 March 2020



Abstract: The self-centering tension-only brace (SC-TOB) is a new and innovative bracing system that provides both a flag-shaped recentering hysteresis and load mitigation to structures. This paper presents an extensive investigation of the nonlinear seismic response of multistory steel frames built with SC-TOBs to internal force, drift, and energy dissipation. Pushover analysis subjected to two lateral load distributions and nonlinear dynamic analysis under ground motion ensembles corresponding to four hazard levels were conducted. The SC-TOBs can be designed to serve as conventional tension-only braces (TOBs) only providing lateral stiffness during minor earthquakes, to function with energy dissipation as intensity increases, and to fully recenter a structure even after severe earthquakes. The findings show that with an increase in the earthquake intensity, both the force response and drift response of the SC-TOB frames (SC-TOBFs) increased; however, the force distribution and drift distribution shapes of the SC-TOBFs remained almost constant. The SC-TOBFs generally experienced more energy dissipation in the lower parts of the building, while the upper stories dissipated almost no energy under certain load conditions, suggesting that the bracings on those stories could be replaced by conventional TOBs for economy. It is demonstrated that the SC-TOBs have immense potential to effectively improve seismic resilience to structures such that rehabilitation costs and operational disruptions after earthquakes are minimized.

Keywords: self-centering; tension-only; brace; damping systems; seismic response; resilience

1. Introduction

Although conventional earthquake-resistant systems (e.g., ductile moment frames, braced frames, or concrete shear walls) designed conforming to current seismic codes are confirmed to achieve life safety and collapse prevention performances, there is wide consensus emerging within the structural engineering community that preventing collapse is simply not sufficient for a more resilient structure. Because those systems are prone to permanent, nonrecoverable deformations (residual deformations) after a significant seismic event, leading to substantial losses associated with costs of rehabilitation and operational disruption. For example, many structures that suffered damage in the 2011 Christchurch Earthquake had to be demolished because of excessive residual deformations even though they had not collapsed [1]. A study by McCormick et al. suggested that for buildings with residual drift greater than 0.5%, it is more economical to demolish and reconstruct them than repair them [2].

To address this drawback with residual deformations, a novel category of seismic-resilient structural system (SRSS) was developed. A typical SRSS generally employs a restoring force mechanism to achieve self-centering (SC), in conjunction with an energy dissipation (ED) mechanism to protect the primary structure. The main approaches to SC can be classified into four categories: rocking systems,

post-tensioned moment frames, shape memory alloy (SMA)-based components, and self-centering braces (SCBs).

The key aspect of rocking systems, including rocking walls [3,4] and rocking braced frames [5,6], is the gap-opening mechanism taking place between the structure and foundation, which softens the structural lateral response without any residual deformations. The gap-opening mechanism can also be applied to beam-column interface to form a post-tensioned moment frame in which the beam is compressed to the side of a column by using post-tensioning (PT) technology [7,8]. However, both rocking systems and post-tensioned frames may suffer from issues of installation complexity and deformation incompatibility [5,9]. Superelastic SMAs, characterized by inherent hysteretic damping and spontaneous recentering, have currently emerged as one class of smart materials for achieving SRSS. Various types of SMA-based components, such as connections, dampers, and braces have been proposed [10–12].

In the family of SRSSs, SCBs are a promising candidate because of their satisfactory SC capability and especially because SC can be developed within the brace elements such that deformation incompatibility can be avoided, and conventional field techniques are sufficient for installation and replacement. Christopoulos et al. [13] were among the pioneers to develop self-centering energy dissipative (SCED) braces. Erochko et al. [14] conducted a shake table test to confirm the behavior of SCED braces within structural systems. Wiebe and Christopoulos [15] adopted Bézier curves to mitigate the sharp stiffness transition in the hysteresis. Karavasilis et al. [16] developed a new nonlinear model for seismic analysis of structures with SCBs. To further improve the recentering capacity, two types of SC-enhanced brace configurations incorporating multiple SC systems, that is, the dual-core SCB [17–20] and the telescoping SCED brace [21,22], were developed independently. More recently, pre-pressed disc springs have been utilized to develop SC, by which the limitations in deformability can be improved further [23–25]. Comparative studies of SCB frames (SCBFs) and buckling-restrained braced (BRB) frames, however, revealed that amplified seismic demands have emerged as a major concern to SCBFs owing to moderate ED capacity depending on the flag-shaped hysteresis loop of SCBs, which was not as full as that of BRBs [26].

Unlike those rigid SCBs, tension-only braces (TOBs) are flexible and can enable the full use of tensile strength of high strength materials without compressive-flexural buckling, thereby reducing the axial stiffness as well as the cross-sectional dimensions of the brace significantly [27,28]. As a result, a mitigating seismic response can be obtained due to the elongated fundamental period of vibration of the resulting structure. In addition, TOBs are lighter in weight, making them easier to install and relatively simple to replace. In view of this, the authors developed a self-centering tension-only brace (SC-TOB) system, in consideration of the load mitigation characteristics of TOBs, to reduce the seismic demands of SCB structures [29]. Several response parameters were studied to compare the behavior of the SC-TOBFs and BRB frames [30].

This study investigated how the SC-TOB can be implemented in multistory steel frames to improve seismic performance in terms of internal force, drift, and energy dissipation. Pushover analysis subjected to two lateral load distributions and nonlinear dynamic analysis under ground motion ensembles scaled to four hazard levels were performed.

2. Analytical Model of SC-TOBFs

2.1. Mechanics of SC-TOB

Figure 1a illustrates the schematic of the SC-TOB system [27,28], which employs a set of PT tendons (shown as a whole unit, for illustrative purposes) to provide a restoring force to achieve self-centering, a frictional device to dissipate seismic input energy, and a high strength steel (HSS) cable as the main bracing element. One end of the PT tendon is anchored to the blocking plate, and the other end is passed around the pulley and connected with the frictional device after pre-tensioning it. The pulley within the SC-TOB is adopted to reduce the strain by half on the PT tendons, if the same

elongation occurs, leading to a double elongation capacity of the bracing system. The mechanics of the SC-TOB system can be explained using an analytical model as presented in Figure 1b, wherein k_t , k_f , and $k_c =$ the axial stiffnesses of the PT tendons, frictional device, and HSS cable, respectively; $F =$ the frictional resistance provided by the frictional device; and $T_{t,0} =$ the pre-tension of the PT tendons. R represents the blocking plate to restrict the left movement of the frictional device.

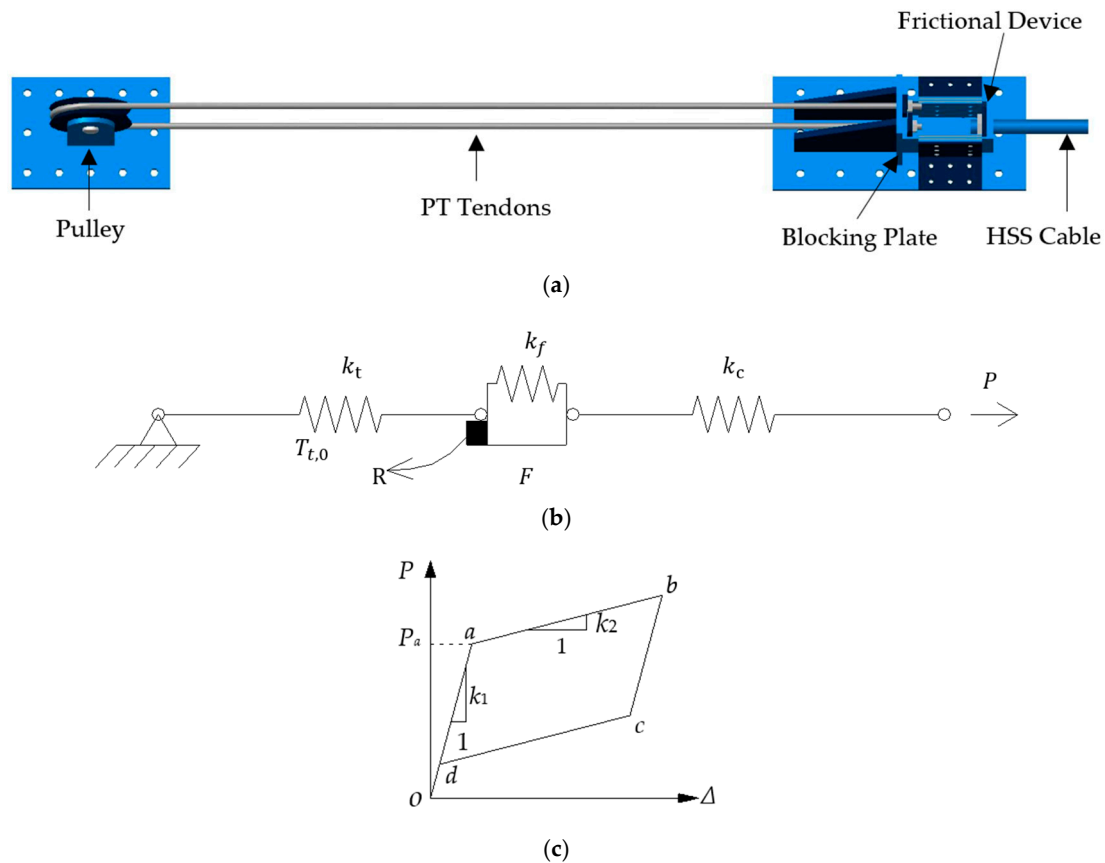


Figure 1. Self-centering tension-only brace (SC-TOB) system: (a) schematic; (b) analytical model; and (c) hysteretic behavior [27,28].

Figure 1c depicts the flag-shaped hysteresis of the SC-TOB. When the load P is too small to overcome the sum of $T_{t,0}$ and F , only the HSS cable works at *stage o-a*, hence the initial stiffness of the SC-TOB, k_1 , is equal to k_c . As P increases to reach the activation load P_a , given by $P_a = T_{t,0} + F$, the PT tendons start to stretch, and meanwhile the energy dissipation mechanism is activated. At *stage a-b*, the axial stiffness of the SC-TOB decreases from k_1 to the post-activation stiffness k_2 , given by $k_2 = (k_t^{-1} + k_f^{-1} + k_c^{-1})^{-1}$. Upon unloading, the friction device is locked, with the friction value varying from F at *event b* to $-F$ at *event c*. During this stage, as the frictional device remains stationary, the stiffness of the SC-TOB is recovered to k_1 . As P further unloads (*stage c-d*), the SC-TOB is pulled back to its initial position under the influence of the tensioning tendons, and the stiffness is once again reduced to k_2 . With continuous unloading during *stage d-o*, as the movement of the friction device is restricted by the blocking plate, the stiffness of the system once again recovers to k_1 .

2.2. Modeling of an SC-TOBF

A typical steel frame equipped with SC-TOBs subjected to lateral loading, P , is illustrated in Figure 2; the solid line indicates a taut HSS cable experiencing positive elongation, while the dotted line indicates a slack, on stand-by for the load reversal. Note that the pulleys mounted on the beam near the beam-column connections are used to guide the HSS cables, which serves a different purpose from

those within the SC-TOBs. The analytical model is constructed using SAP2000 [31]. Key modeling techniques are as follows:

- Beam and column modeling. The beams and columns are modeled using frame elements, which concentrate their inelastic behaviors in nonlinear hinges (lumped plasticity).
- SC-TOB modeling. The multilinear elastic element (MEE) and the multilinear plastic element (MPE) are used to model the nonlinear elastic behavior of PT tendons and the energy dissipation from the frictional device, respectively. For both tendons and frictional device, only the second-stage curves with a softened stiffness of the elements are required; hence, a negligible first-stage deformation has to be specified. For the HSS cable modeling, however, the MEE with a sufficiently long first-stage curve is adopted, because the cable is only permitted to behave in a linear elastic way.
- Pulley modeling. The pulley is modeled using five hinged frame elements within the dotted circle, in which nodes 1, 2, and 3 are located around the center point O. Because a pulley is almost a rigid body in real structures, the axial stiffness of each frame element has to be assigned a sufficiently large value.
- Models assembly. A “body constraint” is specified between nodes O, A, and B, and their vertical projection O', A', and B', respectively, to ensure that each pair of nodes moves together as a 3D rigid body, except that the translational degree of freedom of node A is released to allow its axial movement.

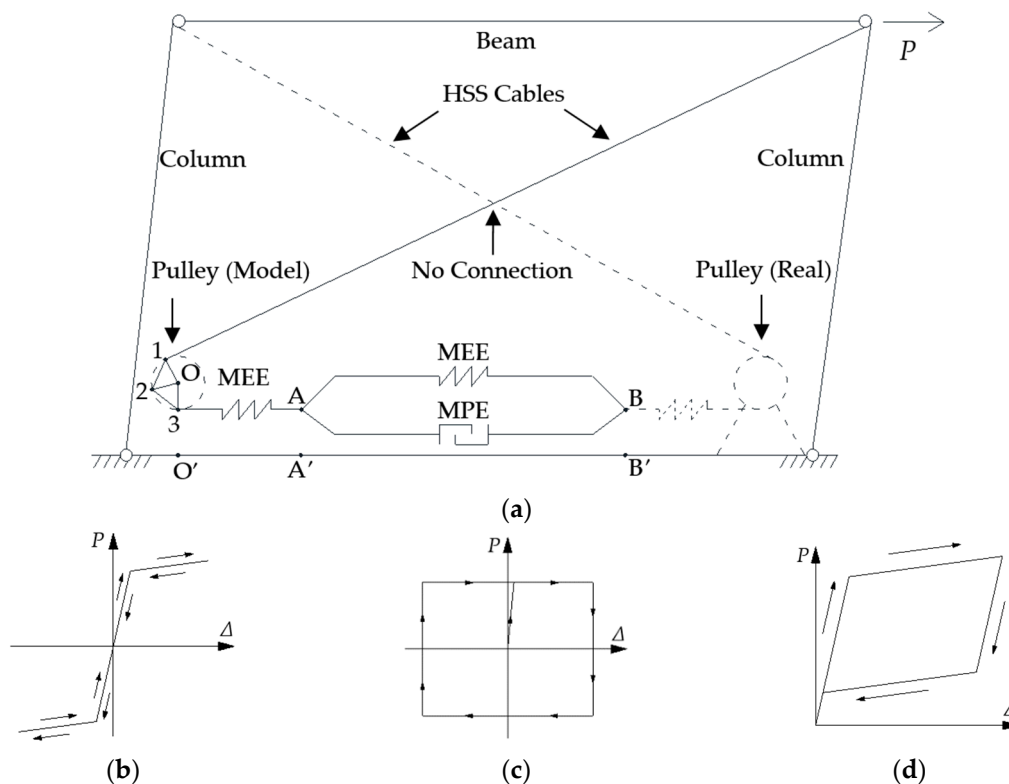


Figure 2. Simulation of the SC-TOB frame (SC-TOBF): (a) SC-TOB arrangement; (b) multilinear elastic element (MEE) hysteresis; (c) multilinear plastic element (MPE) hysteresis; and (d) SC-TOB hysteresis.

2.3. Prototype Building Design

As illustrated in Figure 3, the prototype building is a steel-framed office building with nine stories and five bays, which can be considered as typical of intermediate structures. It has a constant story height of 3.9 m totaling 35.1 m and a constant bay width of 9 m totaling 45 m. Column types 1 to 6 are identified in Figure 3. Nonmoment-resisting beam-column connections are assumed in the design,

because such connections have sufficient rotation capacity to accommodate a large drift demand without damaging the connection region [32]. The building uses four perimeter-braced frames for resisting seismic load in either earthquake direction.

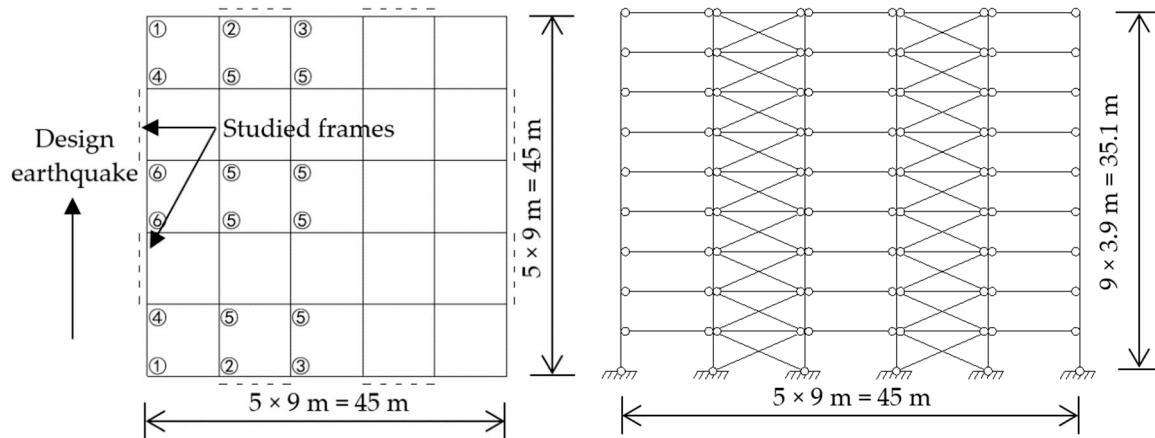


Figure 3. Layouts and load information of the prototype building. Gravity loads: Roof: Dead = 5.0 kPa; Live = 2.0 kPa. Floor: Dead = 4.5 kPa; Live = 4.0 kPa. Exterior walls = 10 kN/m. Seismic load data: Seismic precautionary intensity: 8. Site classification: III. Basic acceleration of ground motion: 0.20 g.

It is assumed that all the seismic energy is dissipated by the SC-TOBs, and the load-resisting elements always remain elastic during an earthquake. The braced bays are designed to resist both gravity loading and lateral seismic loading, whereas the unbraced bays only need to resist gravity loading. The beams and columns are made of Q345 steel having a yield stress of 345 MPa, and the cables are made of HSS strands, with an ultimate strength of 1670 MPa. Geometric nonlinearity is incorporated to consider the P-Delta effects through large displacement analysis. Rayleigh damping is used with inherent 4% critical damping at the first two modes of vibration. The geometric properties of structural elements are selected according to design codes [33–35] as listed in Table 1. All the SC-TOBs used in the prototype building are designed to activate at a story drift angle θ_a of 0.4%, which is consistent with the code-prescribed elastic limit for steel structures [34]. The hysteresis of each type of SC-TOB is depicted in Figure 4.

Table 1. Detailed properties of structural elements in the prototype building.

Story	Unbraced Bays		Braced Bays				
	Beam (mm)	Column (mm)	Beam (mm)	Column (mm)	SC-TOB		
					Cable Diam (mm)	PT Force (kN)	Friction (kN)
7–9	H650 × 300 × 12 × 20	□400 × 400 × 10 × 10	H800 × 300 × 14 × 26	□400 × 400 × 10 × 10	$\varphi = 70$	564.30	537.42
4–6		□400 × 400 × 12 × 12	H850 × 300 × 17 × 31	□450 × 450 × 14 × 14	$\varphi = 80$	737.04	701.94
1–3		□400 × 400 × 16 × 16	H900 × 300 × 16 × 28	□500 × 500 × 18 × 18	$\varphi = 90$	932.83	888.38

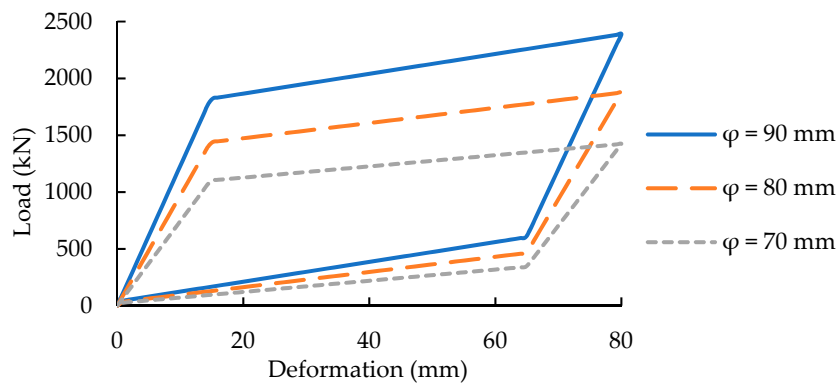


Figure 4. Hysteresis of each type of SC-TOB.

Since pinned beam-to-column connections are assumed in the design, and each column is continuous and pinned at its base, lateral seismic resistance is provided and equally distributed by the two braced frames, along the direction of the earthquake. In view of the symmetrical plan dimensions of the prototype building, the torsion effect can be neglected, thereby allowing for a 2D analysis in lieu of a 3D analysis for efficiency and simplicity (see Figure 5). In the 2D model, the link beams between columns ④ and ① are assumed to act as rigid diaphragms that transfer lateral deformations from braced to unbraced frames. The 2D analytical model is validated to be feasible by the modal analysis comparison as shown in Table 2, and it is therefore used in the following investigations.

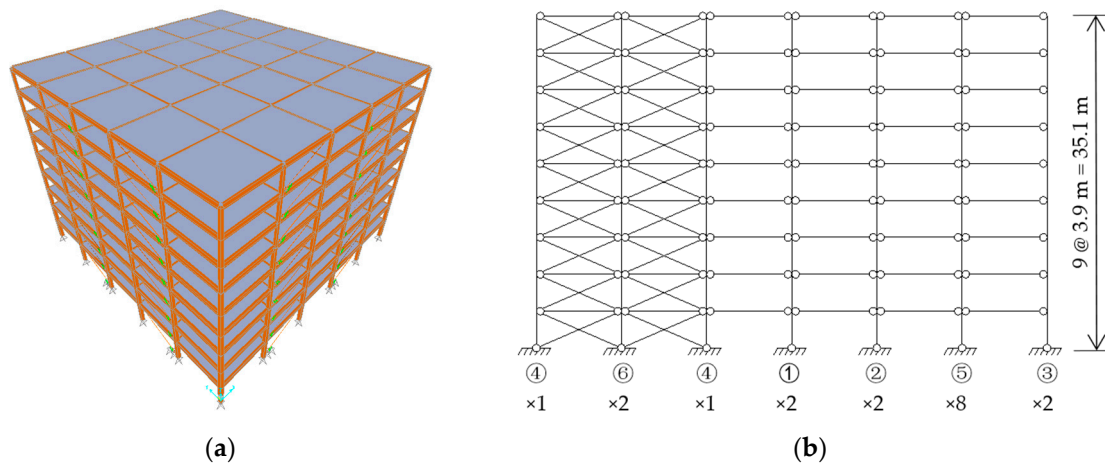


Figure 5. Analytical model of the SC-TOBFs: (a) 3D model and (b) 2D model.

Table 2. Modal analysis comparison.

Model	1st Mode		2nd Mode		3rd Mode	
	Period (s)	MPMR	Period (s)	MPMR	Period (s)	MPMR
3D	2.697	78%	0.920	14%	0.523	4%
2D	2.608	79%	0.903	13%	0.516	4%

MPMR: modal participating mass ratio.

3. Incremental Static (Pushover) Analysis

As illustrated in Figure 6, two suggested lateral load distributions [36], the parabolic distribution (denoted as “LD-P”) and the uniform distribution (denoted as “LD-U”), are adopted for the incremental static analysis. The procedure is performed until a target displacement represented by the roof drift angle, θ_H , reaches 2%, where $\theta_H = \Delta_H/H$, with Δ_H being the roof displacement and H being the building height.

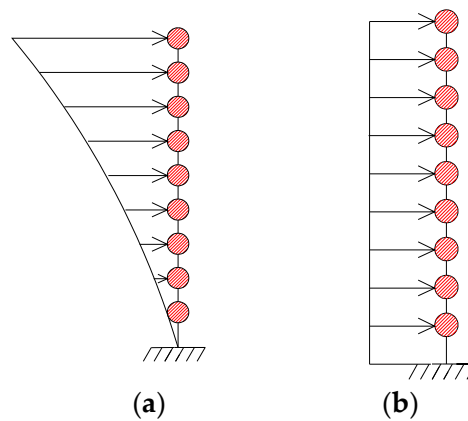


Figure 6. Lateral load distributions: (a) parabolic distribution (LD-P) and (b) uniform distribution (LD-U).

3.1. Force Response

As shown in Figure 7, the SC-TOBFs exhibit a bilinear base shear response with a significant stiffness reduction when the yield-like activation is attained, similar to the softening behavior of yielding systems, facilitating limiting the seismic forces induced in the structures. The activation initiates at $\Delta_H = 200$ mm (corresponding to $\theta_H = 0.57\%$) and $\Delta_H = 150$ mm (corresponding to $\theta_H = 0.43\%$) under LD-P and LD-U, respectively.

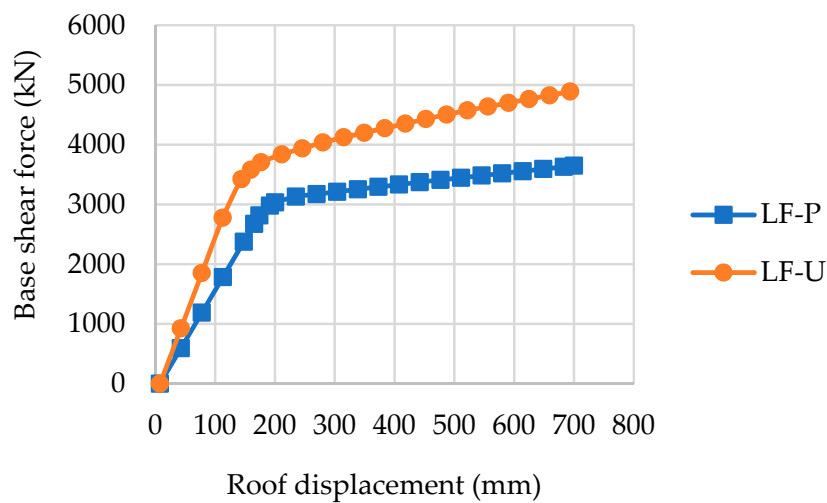


Figure 7. Base shear response.

Figure 8 shows that the axial force in the cables keeps nonlinearly increasing with an increase in Δ_H and decreasing with the building height and that each type of SC-TOB with hysteresis presented in Figure 4 in every three stories shows a similar tendency. It can also be seen that the distribution of the cable axial forces under LD-U is more uniform than that under LD-P.

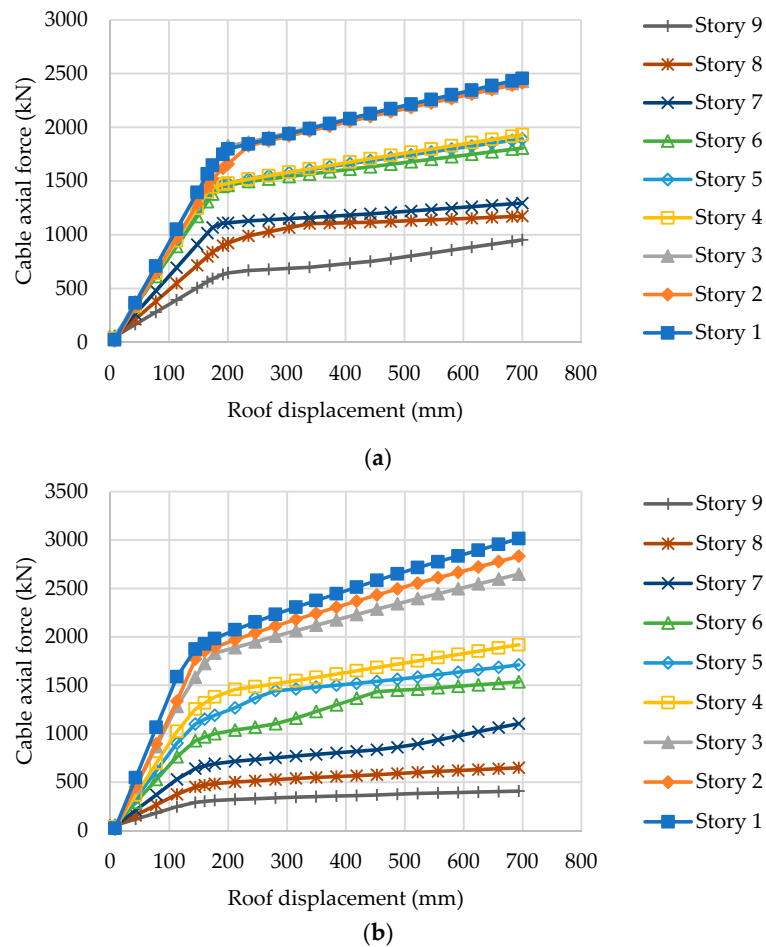


Figure 8. Cable axial force response under (a) LD-P and (b) LD-U.

3.2. Drift Response

As shown in Figure 9, the inter-story drift angle, θ , generally decreases with the building height under both lateral load distributions except that the θ in the 4th story under LD-P is even larger than those in the lowest three stories. This is mainly because the load increment in the middle stories under LD-P is rather small, whereas the lateral stiffness decreases suddenly from the 3rd to the 4th story owing to the changing of SC-TOB type.

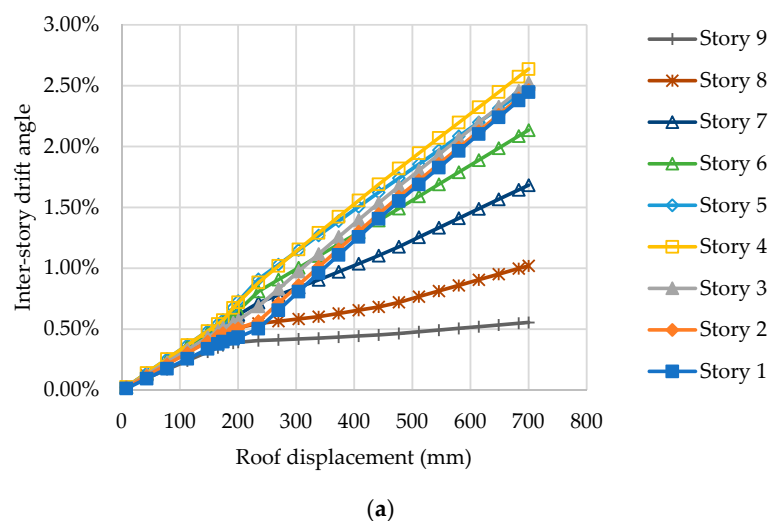


Figure 9. Cont.

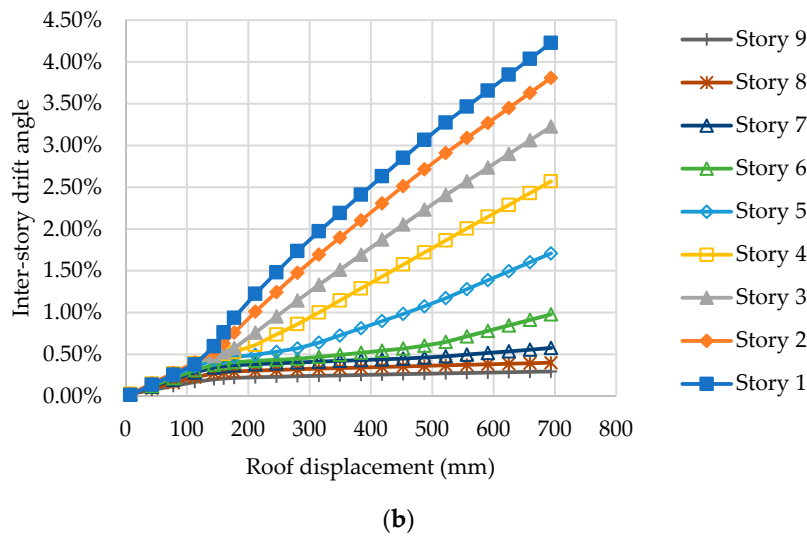


Figure 9. Inter-story drift response under (a) LD-P and (b) LD-U.

3.3. Energy Dissipation

For every single SC-TOB, the energy dissipation $E = F\Delta$, where F is the friction force selected according to brace type from Table 1, and Δ is the slip displacement, which equals to the corresponding elongation of MPE. As shown in Figure 10, the seismic energy dissipated in each story stably increases with increasing roof drift once the relevant SC-TOBs are activated with a θ equal to or slightly greater than 0.4% as designed.

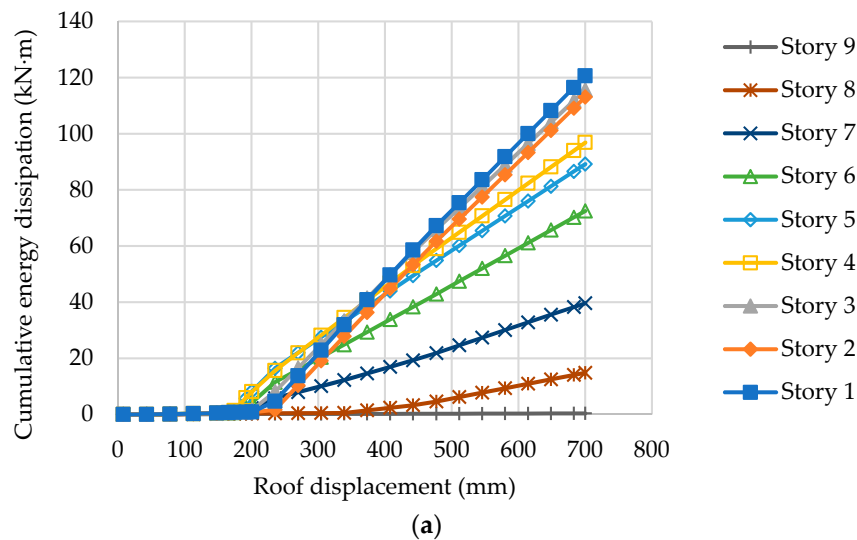


Figure 10. Cont.

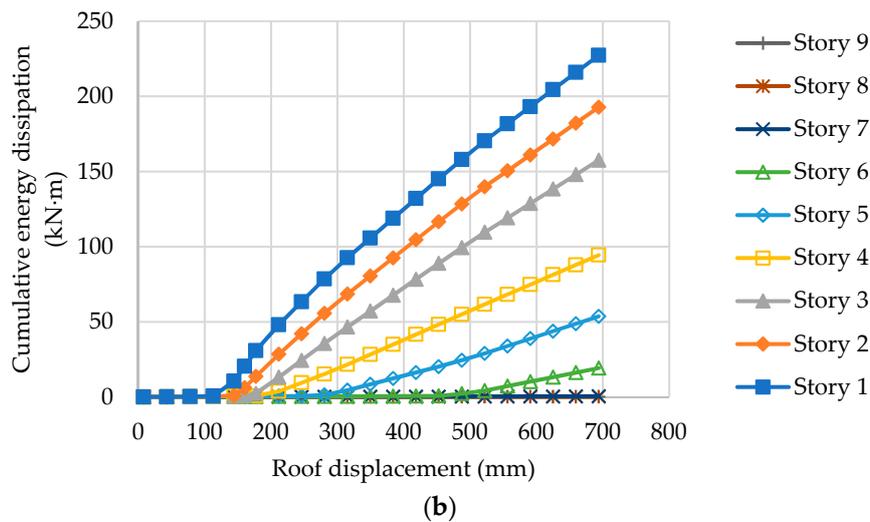


Figure 10. Cumulative energy dissipation response under (a) LD-P and (b) LD-U.

Figure 11 counts the cumulative energy dissipated in each story under both load distributions. The lower stories generally dissipate more seismic energy than the middle and higher stories do, with almost no energy dissipation observed in the top story under LD-P and top three stories under LD-U, suggesting that SC-TOBs on those stories could be replaced by conventional TOBs without influencing the self-centering capability. Although the energy dissipation distributions are quite different, being more uniform under LD-P, the cumulative dissipations are not significantly different: 664.15 kN·m for LD-P is 88.47% of that for LD-U (750.71 kN·m).

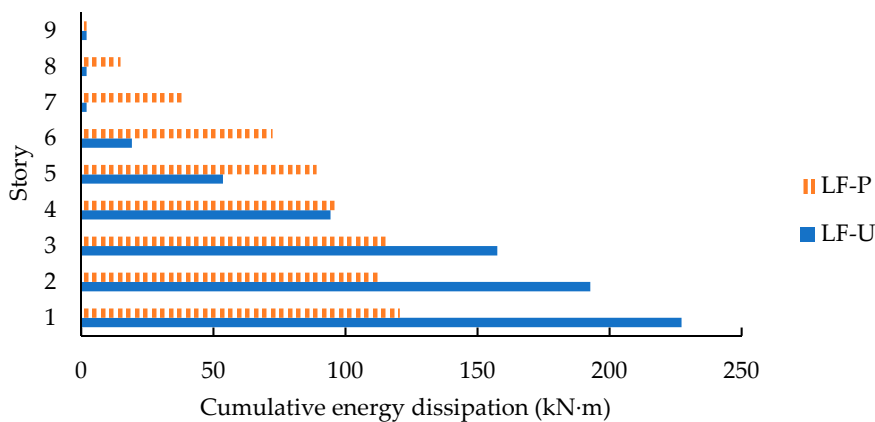


Figure 11. Cumulative energy dissipation in each story.

4. Nonlinear Dynamic Analysis

4.1. Ground Motion

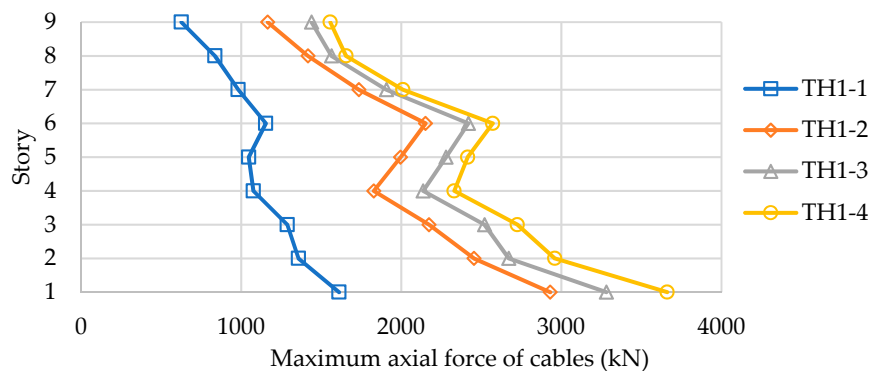
One artificial and three real suites of ground motions (GMs), as listed in Table 3, were selected corresponding to the site class (III, characteristic period 0.45 s) for the time history analysis. Each GM is scaled to four hazard levels, with a peak ground acceleration of 0.07 g, 0.22 g, 0.41 g, and 0.52 g, representing frequently occurred earthquake (FOE) with a return period of approximately 50 years, design basis earthquake (DBE) with a return period of approximately 500 years, maximum considered earthquake (MCE) with a return period of approximately 2500 years, and extremely rare earthquake (ERE) with an intensity value of 0.5 greater than that of MCE, respectively.

Table 3. Ground motion properties for nonlinear dynamic analysis (4 suites of 16 excitations).

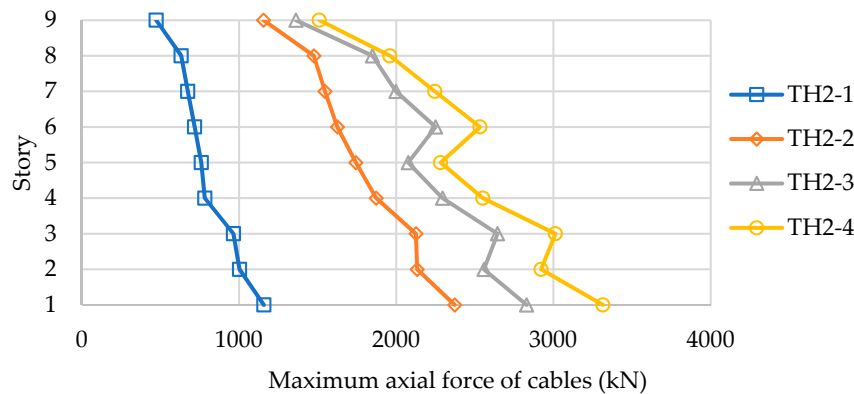
Suite No.	Earthquake	Duration (s)	Peak Ground Acceleration (g)				
GM 1	El-Centro 1940	53.4	Origin 0.35	TH1-1 0.07	TH1-2 0.22	TH1-3 0.41	TH1-4 0.52
GM 2	Taft 1952	54.2	Origin 0.16	TH2-1 0.07	TH2-2 0.22	TH2-3 0.41	TH2-4 0.52
GM 3	Tianjin 1976	19.2	Origin 0.15	TH3-1 0.07	TH3-2 0.22	TH3-3 0.41	TH3-4 0.52
GM 4	Artificial	30.0	Origin 0.10	TH4-1 0.07	TH4-2 0.22	TH4-3 0.41	TH4-4 0.52

4.2. Force Response

Figure 12 shows the maximum response envelopes of the axial force of cable under each seismic excitation. The envelop shapes under FOE conditions are dependent on the SC-TOBs activation to “yield.” For example, TH2-1 and TH4-1 envelops are nearly linear, indicating that braces have not been fully activated at that time. With an increase in the intensity from DBE to ERE, all the braces are gradually activated; thus, the other three envelopes under each GM exhibit the same tendency. As the SC-TOB type varies every three stories, the location where the maximum cable forces appear in the lower, middle, and higher parts of the building are the 1st, 6th, and 7th stories, respectively, under GMs 1-3, and the 1st, 4th, and 8th stories, respectively, under GM 4. A final strength check process reflects that all the bracings remain elastic without damage even under MCE and ERE, as presented in Table 4.



(a)



(b)

Figure 12. Cont.

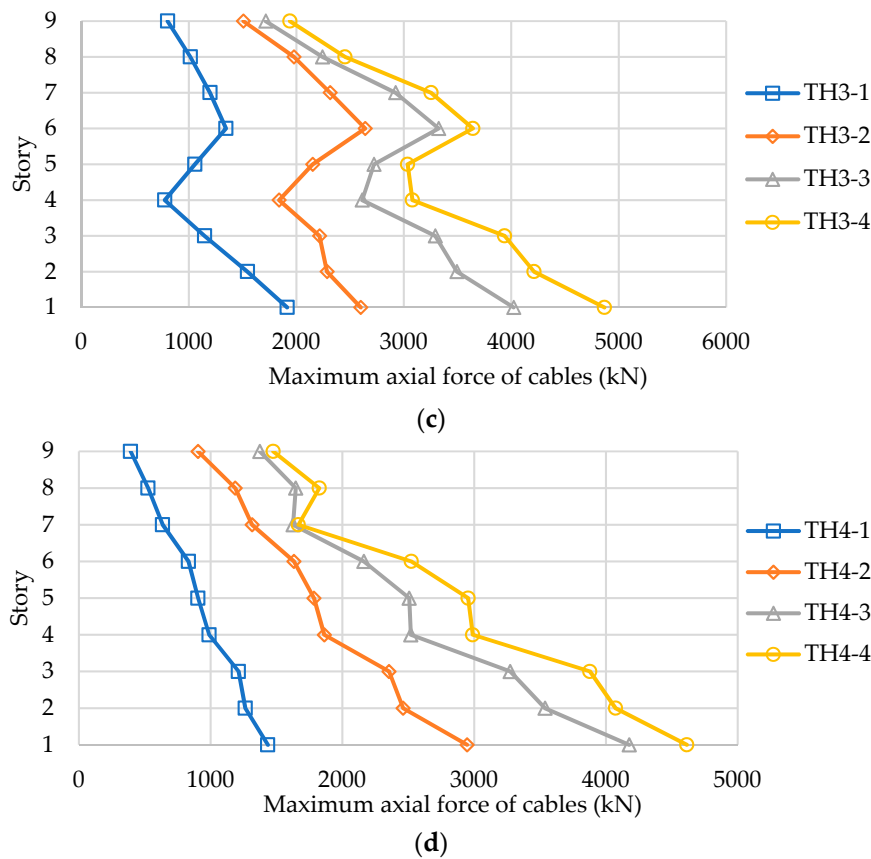


Figure 12. Maximum response envelopes of cable axial force under (a) GM 1; (b) GM 2; (c) GM 3; and (d) GM4.

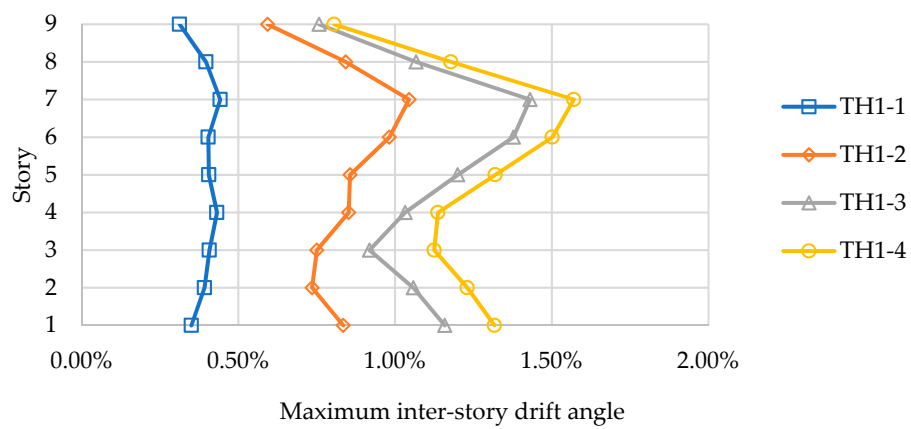
Table 4. Maximum axial force of cables under GMs 1-4.

Story	Suite No.	MCE (kN)	ERE (kN)	Design Value (kN)
7-9	GM 1	1907	2010	3384
	GM 2	1998	2245	
	GM 3	2922	3253	
	GM 4	1666	1825	
4-6	GM 1	2419	2517	4421
	GM 2	2294	2550	
	GM 3	3324	3643	
	GM 4	2519	2989	
1-3	GM 1	3281	3661	5595
	GM 2	2829	3315	
	GM 3	4022	4867	
	GM 4	4176	4614	

4.3. Drift Response

Figure 13 shows the maximum response envelopes of inter-story drift angle θ along the height. As shown, the drift angles are basically uniform within the code-prescribed elastic limit 0.4% under FOE excitations, except that exceeding values appear on 6th, 7th, and 8th stories under TH3-1, indicating that the SC-TOBs on those stories are working in advance than designed. Under DBE and MCE excitations, all the SC-TOBs are functioning as expected as a result of $\theta > \theta_a = 0.4\%$, dissipating seismic energy and protecting the primary structure. The occurrence of maximum θ begins on the 7th story for GMs 1-3, and on the 1st story for GM 4, respectively, neither of which is greater or just slightly greater than the plastic limit of 2.0%. The drift mode continues to develop when subjected to the ERE

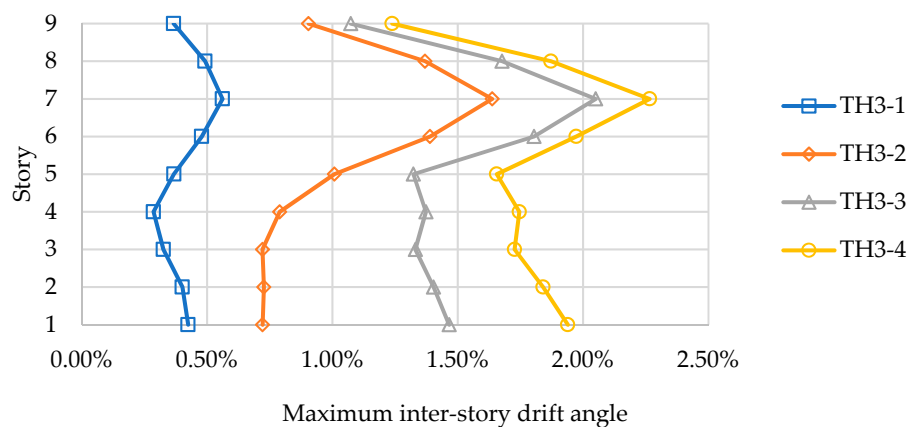
excitations, but the maximum values in TH1-4 and TH2-4 are still within the plastic limit 2.0%, while 1.14 and 1.20 times the plastic limit in TH3-4 and TH4-4, respectively.



(a)



(b)



(c)

Figure 13. Cont.



(d)

Figure 13. Maximum response envelopes of inter-story drift under (a) GM 1; (b) GM 2; (c) GM 3; and (d) GM4.

4.4. Energy Dissipation

The cumulative energy dissipation of each SC-TOB can be computed using the approach presented in Section 3.3. However, a noteworthy difference is that the slip displacement Δ . is the summation of differences between every two analysis steps when performing dynamic analysis, i.e., $\Delta = \sum_{m=0}^{n-1} |\Delta_{m+1} - \Delta_m|$, where Δ_m represents the MLP elongation at the m^{th} analysis step and can be extracted from its elongation time history.

Figure 14 counts the cumulative energy dissipated by each type of SC-TOB adopted in the lower, middle, and higher stories of the prototype building, respectively, under 16 seismic excitations. As illustrated, no energy dissipation is observed under all FOE conditions, indicating that the SC-TOBs are working as conventional TOBs only providing necessary lateral stiffness. With the increasing intensity of ground motions from DBE, energy dissipation is initiated and enhanced continuously without stagnating at certain stories of the structure, reflecting good interoperability of the SC-TOBs along the building height. It is also revealed that the lower and middle stories dissipate much more energy than the upper stories do. The total cumulative energy dissipation of the SC-TOBFs is given in Figure 15.

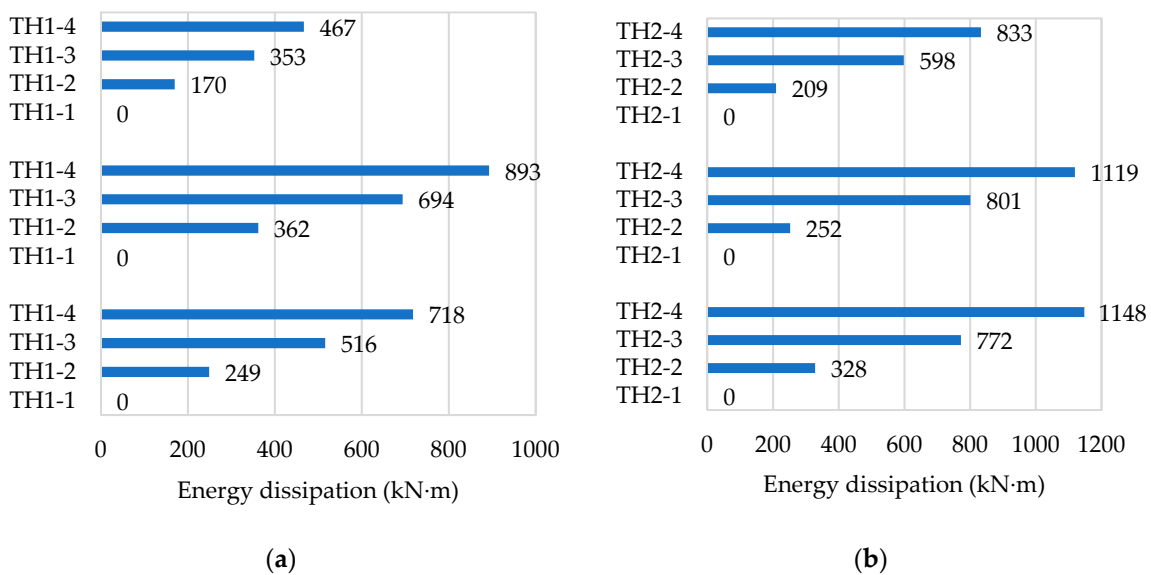


Figure 14. Cont.

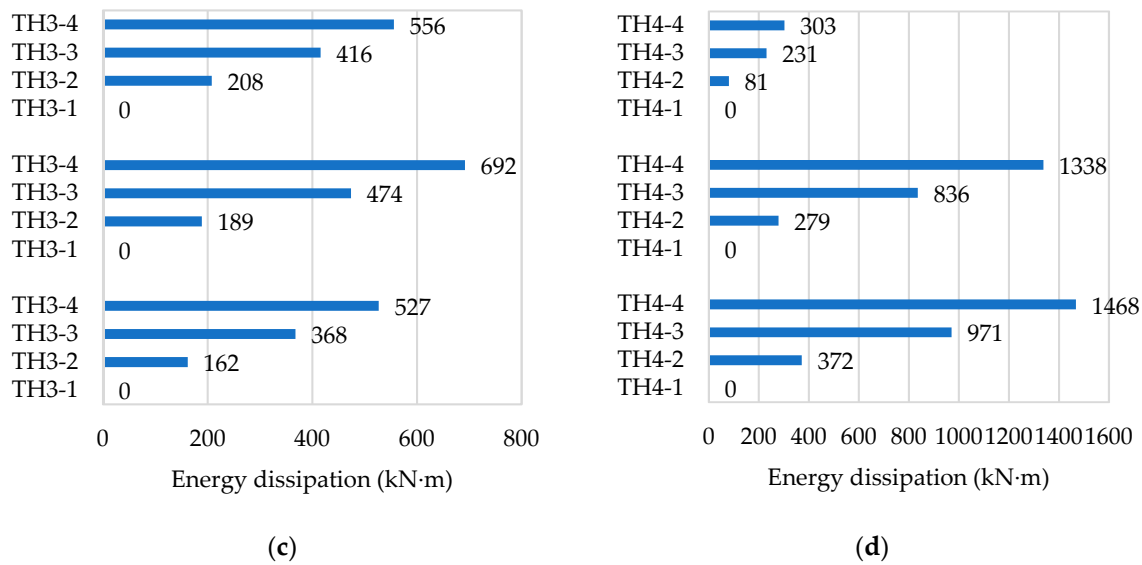


Figure 14. Energy dissipation distributions under (a) GM 1; (b) GM 2; (c) GM 3; and (d) GM 4.

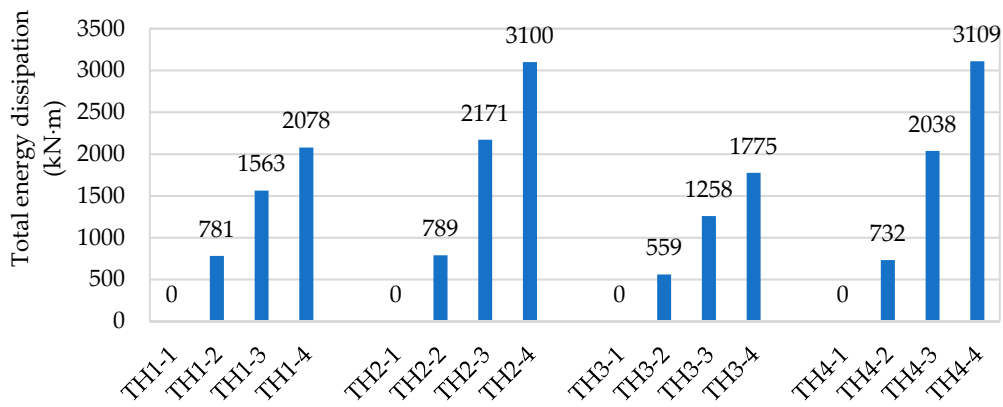


Figure 15. Total cumulative energy dissipation.

5. Conclusions

This work presents an extensive investigation of the nonlinear seismic response of multistory steel frames built with self-centering tension-only braces (SC-TOBs) to internal force, drift, and energy dissipation. Pushover analysis adopting two lateral load distributions and nonlinear dynamic analysis under four suites of 16 ground motions corresponding to four hazard levels were conducted. The conclusions from the investigation can be summarized as follows:

- As expected, the SC-TOBs serve as conventional TOBs only providing necessary lateral stiffness when subjected to low level seismic hazard and begin to function with energy dissipation as the intensity of ground motions increases. All structural elements, such as cables, always remain elastic both in pushover analysis within 2% roof drift angle and in dynamic analysis under the severe hazard level, displaying a full self-centering capability without any residual deformations.
- The SC-TOB frames (SC-TOBFs) exhibit a bilinear base shear response with a significant stiffness reduction when the yield-like activation is attained, which facilitates the capping of seismic forces induced in the structures similar to the softening behavior of yielding systems. Besides, the internal force distributions of structural elements are observed to be nearly identical with the increase of intensity as long as the SC-TOBs are triggered.
- Although drift is prone to be concentrated around the middle stories of the SC-TOBFs when subjected to parabolic load distribution and at bottom stories under uniform load distribution, it is

reliably limited within the code-prescribed limit of 2.0% under maximum considered earthquakes, and the SC-TOBFs are confirmed to have full self-centering capacity even when the maximum inter-story drift angle reaches twice the limit. In addition, the drifts develop as the intensity increases, but their distribution remains nearly unchanged.

- With the intensity getting higher, the energy dissipation of the SC-TOBFs continuously increases without stagnating at certain stories of the building, reflecting good structural interoperability of the bracing members along the structure height. For the prototype building, the lower and middle stories generally dissipate more seismic energy than the upper stories, and almost no energy is dissipated in the upper stories under certain load conditions, suggesting that the SC-TOBs on those stories could be replaced by conventional TOBs, thereby reducing costs while retaining fully the self-centering capability.

Author Contributions: Conceptualization, P.C. and J.D.; Formal analysis, P.C. and W.T.; Funding acquisition, P.C. and D.C.; Writing—original draft, P.C. and W.T.; Writing—review & editing, J.D. and D.C. All authors have read and agreed to the published version of the manuscript.

Funding: This research was funded by the National Natural Science Foundation of China (Grants No. 51708482 and No. 51578478), the China Postdoctoral Science Foundation (Grant No. 2017M621593), and the Six Talent Peaks Project in Jiangsu Province (Grant No. JZ-035).

Conflicts of Interest: The authors declare no conflict of interest.

References

1. Bruneau, M.; MacRae, G. *Reconstructing Christchurch: A Seismic Shift in Building Structural Systems*; The Quake Centre, University of Canterbury: Christchurch, New Zealand, 2017; pp. 24–52.
2. McCormick, J.; Aburano, H.; Ikenaga, M.; Nakashima, M. Permissible residual deformation levels for building structures considering both safety and human elements. In Proceedings of the 14th World Conference on Earthquake Engineering, Beijing, China, 12–17 October 2008.
3. Holden, T.; Restrepo, J.; Mander, J.B. Seismic performance of precast reinforced and prestressed concrete walls. *J. Struct. Eng.* **2003**, *129*, 286–296. [[CrossRef](#)]
4. Kovacs, M.A.; Wiebe, L. Controlled rocking CLT walls for buildings in regions of moderate seismicity: Design procedure and numerical collapse assessment. *J. Earthq. Eng.* **2019**, *23*, 750–770. [[CrossRef](#)]
5. Eatherton, M.R.; Hajjar, J.F.; Deierlein, G.G.; Krawinkler, H.; Billington, S.; Ma, X. Controlled rocking of steel-framed buildings with replaceable energy-dissipating fuses. In Proceedings of the 14 World Conference on Earthquake Engineering, Beijing, China, 12–17 October 2008.
6. Bosco, M.; Marino, E.M.; Rossi, P.P. A design procedure for pin-supported rocking buckling-restrained braced frames. *Earthq. Eng. Struct. Dyn.* **2018**, *47*, 2840–2863. [[CrossRef](#)]
7. Ricles, J.; Sause, R.; Garlock, M.; Zhao, C. Posttensioned seismic-resistant connections for steel frames. *J. Struct. Eng.* **2001**, *127*, 113–121. [[CrossRef](#)]
8. Bojórquez, E.; López-Barraza, A.; Reyes-Salazar, A.; Ruiz, S.E.; Ruiz-García, J.; Formisano, A.; López-Almansa, F.; Carrillo, J.; Bojórquez, J. Improving the structural reliability of steel frames using posttensioned connections. *Adv. Civ. Eng.* **2019**, *2019*, 8912390. [[CrossRef](#)]
9. Garlock, M.E.M.; Li, J. Steel self-centering moment frames with collector beam floor diaphragms. *J. Constr. Steel Res.* **2008**, *64*, 526–538. [[CrossRef](#)]
10. Fang, C.; Yam, M.C.H.; Lam, A.C.C.; Xie, L.K. Cyclic performance of extended end-plate connections equipped with shape memory alloy bolts. *J. Constr. Steel Res.* **2014**, *94*, 122–136. [[CrossRef](#)]
11. Seo, J.; Kim, Y.C.; Hu, J.W. Pilot study for investigating the cyclic behavior of slit damper systems with recentering shape memory alloy (SMA) bending bars used for seismic restrainers. *Appl. Sci.* **2015**, *5*, 187–208. [[CrossRef](#)]
12. Hu, J.W.; Noh, M.H.; Ahn, J.H. Experimental investigation on the behavior of bracing damper systems by utilizing metallic yielding and recentering material devices. *Adv. Mater. Sci. Eng.* **2018**, *2018*, 2813058. [[CrossRef](#)]
13. Christopoulos, C.; Tremblay, R.; Kim, H.J.; Lacerte, M. Self-centering energy dissipative bracing system for the seismic resistance of structures: Development and validation. *J. Struct. Eng.* **2008**, *134*, 96–107. [[CrossRef](#)]

14. Erochko, J.; Christopoulos, C.; Tremblay, R.; Kim, H.J. Shake table testing and numerical simulation of a self-centering energy dissipative braced frame. *Earthq. Eng. Struct. Dyn.* **2013**, *42*, 1617–1635. [[CrossRef](#)]
15. Wiebe, L.; Christopoulos, C. Using bézier curves to model gradual stiffness transitions in nonlinear elements: Application to self-centering systems. *Earthq. Eng. Struct. Dyn.* **2011**, *40*, 1535–1552. [[CrossRef](#)]
16. Karavasilis, T.L.; Blakeborough, T.; Williams, M.S. Development of nonlinear analytical model and seismic analyses of a steel frame with self-centering devices and viscoelastic dampers. *Comput. Struct.* **2011**, *89*, 1232–1240. [[CrossRef](#)]
17. Chou, C.C.; Chung, P.T. Development of cross-anchored dual-core self-centering braces for seismic resistance. *J. Constr. Steel Res.* **2014**, *101*, 19–32. [[CrossRef](#)]
18. Chou, C.C.; Chen, Y.C.; Pham, D.H.; Truong, V.M. Steel braced frames with dual-core SCBs and sandwiched BRBs: Mechanics, modeling and seismic demands. *Eng. Struct.* **2014**, *72*, 26–40. [[CrossRef](#)]
19. Chou, C.C.; Chen, Y.C. Development of Steel Dual-Core Self-Centering Braces: Quasi-Static Cyclic Tests and Finite Element Analyses. *Earthq. Spectra* **2015**, *31*, 247–272. [[CrossRef](#)]
20. Chou, C.C.; Wu, T.H.; Beato, A.R.O.; Chung, P.T.; Chen, Y.C. Seismic design and tests of a full-scale one-story one-bay steel frame with a dual-core self-centering brace. *Eng. Struct.* **2016**, *111*, 435–450. [[CrossRef](#)]
21. Kammula, V.; Erochko, J.; Kwon, O.S.; Christopoulos, C. Application of hybrid-simulation to fragility assessment of the telescoping self-centering energy dissipative bracing system. *Earthq. Eng. Struct. Dyn.* **2014**, *43*, 811–830. [[CrossRef](#)]
22. Erochko, J.; Christopoulos, C.; Tremblay, R. Design and testing of an enhanced-elongation telescoping self-centering energy-dissipative brace. *J. Struct. Eng.* **2015**, *141*, 04014163. [[CrossRef](#)]
23. Xu, L.H.; Fan, X.W.; Li, Z.X. Development and experimental verification of a pre-pressed spring self-centering energy dissipation brace. *Eng. Struct.* **2016**, *127*, 49–61. [[CrossRef](#)]
24. Xu, L.H.; Fan, X.W.; Li, Z.X. Hysteretic analysis model for pre-pressed spring self-centering energy dissipation braces. *J. Struct. Eng.* **2018**, *144*, 04018073. [[CrossRef](#)]
25. Xu, L.H.; Yao, S.Q.; Sun, Y.S. Development and validation tests of an assembly self-centering energy dissipation brace. *Soil Dyn. Earthq. Eng.* **2019**, *116*, 120–129. [[CrossRef](#)]
26. Qiu, C.X.; Zhu, S.Y. High-mode effects on seismic performance of multi-story self-centering braced steel frames. *J. Constr. Steel Res.* **2016**, *119*, 133–143. [[CrossRef](#)]
27. Papagiannopoulos, G.A. On the seismic behaviour of tension-only concentrically braced steel structure. *Soil Dyn. Earthq. Eng.* **2018**, *115*, 27–35. [[CrossRef](#)]
28. Mousavi, S.A.; Zahrai, S.M. Contribution of pre-slacked cable braces to dynamic stability of non-ductile frames; an analytical study. *Eng. Struct.* **2016**, *117*, 305–320. [[CrossRef](#)]
29. Chi, P.; Guo, T.; Peng, Y.; Cao, D.F.; Dong, J. Development of a self-centering tension-only brace for seismic protection of frame structures. *Steel Comp. Struct.* **2018**, *26*, 573–582.
30. Chi, P.; Tian, W.L.; Guo, T.; Cao, D.F.; Dong, J. Parametric study on the seismic response of steel-framed buildings with self-centering tension-only braces. *Adv. Civ. Eng.* **2019**, *2019*, 9204362. [[CrossRef](#)]
31. SAP2000. *Structural Analysis Program, Version 17.3.0*; Computers and Structures, Inc.: Berkeley, CA, USA, 2015.
32. Fahnstock, L.A.; Ricles, J.M.; Sause, R. Experimental evaluation of a large-scale buckling-restrained braced frame. *J. Struct. Eng.* **2007**, *133*, 1205–1214. [[CrossRef](#)]
33. FEMA 450. *NEHRP Recommended Provisions for Seismic Regulations for New Buildings and Other Structures: Part 1-Provisions and Part 2-Commentary*; FEMA: Washington, DC, USA, 2003.
34. GB 50011-2010. *Code for Seismic Design of Buildings*; Ministry of Housing and Urban-Rural Development of China: Beijing, China, 2010.
35. AISC 341-16. *Seismic Provisions for Structural Steel Buildings*; American Institute of Steel Construction: Chicago, IL, USA, 2016.
36. ASCE 7-10. *Minimum Design Loads for Buildings and Other Structures*; American Society of Civil Engineers: Reston, VA, USA, 2010.

